THE JOURNAL OF PHYSICAL CHEMISTRY Letters

Letter

Cite This: J. Phys. Chem. Lett. 2018, 9, 364−372

pubs.acs.org/JPCL

Photophysical and Fluorescence Anisotropic Behavior of Polyfluorene β-Conformation Films

Meng-Na Yu,[†] Hamid Soleimaninejad,[‖] Jin-Yi Lin,*[,§] Zong-Yan Zuo,[†] Bin Liu,[†] Yi-Fan Bo,[†] Lu-Bing Bai,[§] Ya-Min Han,[§] Trevor A. Smith,*[,‖] Man Xu,[§] Xiang-Ping Wu,[†] Dave E. Dunstan,[⊥] Rui-Dong Xia,[†] Ling-Hai Xie,*[,†] Donal D. C. Bradley,[#] and Wei Huang*[,†,‡,§]

[†]Centre for Molecular Systems and Organic Devices (CMSOD), Key Laboratory for Organic Electronics and Information Displays & Jiangsu Key Laboratory for Biosensors, Institute of Advanced Materials (IAM), Jiangsu National Synergetic Innovation Center for Advanced Materials (SICAM), Nanjing University of Posts & Telecommunications, 9 Wenyuan Road, Nanjing 210023, China

[‡]Shaanxi Institute of Flexible Electronics (SIFE), Northwestern Polytechnical University (NPU), 127 West Youyi Road, Xi'an 710072, Shaanxi, China

[§]Key Laboratory of Flexible Electronics (KLOFE) & Institute of Advanced Materials (IAM), Jiangsu National Synergetic Innovation Center for Advanced Materials (SICAM), Nanjing Tech University (NanjingTech), 30 South Puzhu Road, Nanjing 211816, China

[‖]ARC Centre of Excellence in Exciton Science, School of Chemistry, The University of Melbourne, Parkville, Victoria 3010, Australia

[⊥]Department of Chemical and Biomolecular Engineering, The University of Melbourne, Parkville, Victoria 3010, Australia

[#]Departments of Engineering Science and Physics and Division of Mathematical, Physical and Life Sciences, Oxford University, 9 Parks Road, Oxford OX1 3PD, United Kingdom

Supporting Information

ABSTRACT: We demonstrate a systematic visualization of the unique photophysical and fluorescence anisotropic properties of polyfluorene coplanar conformation (β-conformation) using time-resolved scanning confocal fluorescence imaging (FLIM) and fluorescence anisotropy imaging microscopy (FAIM) measurements. We observe inhomogeneous morphologies and fluorescence decay profiles at various micrometer-sized regions within all types of polyfluorene β-conformational spin-coated films. Poly(9,9-dioctylfluorene-2,7-diyl) (PFO) and poly[4-(octyloxy)-9,9-diphenylfluoren-2,7-diyl]-*co*-[5-(octyloxy)-9,9-diphenylfluoren-2,7-diyl] (PODPF) β-domains both have shorter lifetime than those of the glassy conformation for the longer effective conjugated length and rigid chain structures. Besides, β-conformational regions have larger fluorescence anisotropy for the low molecular rotational motion and high chain orientation, while the low anisotropy in glassy conformational regions shows more rotational freedom of the chain and efficient energy migration from amorphous regions to β-conformation as a whole. Finally, ultrastable ASE threshold in the PODPF β-conformational films also confirms its potential application in organic lasers. In this regard, FLIM and FAIM measurements provide an effective platform to explore the fundamental photophysical process of conformational transitions in conjugated polymer.

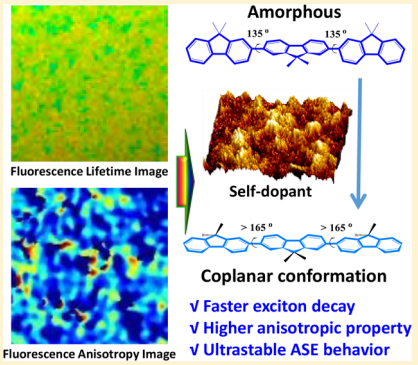

Conjugated polymers are materials that have demonstrated use for emerging optoelectronic applications.[1−3] The sp^2 p_z orbital hybridization and overlap of the carbon atoms along the conjugated backbone afford chain effective and enhanced delocalization of the electronic wave functions, which can control the polymer properties of charge-transport and neutral excited species.[2] Consequently, programmable chain conformation is a key tool to control their optical and electronic properties, such as absorption, emission, and conductivity, and especially allow for their anisotropy because of the intrinsic directional p-orbital overlap and π-electron delocalization along the conjugated backbone.[4,5] Besides, conjugated polymers are weakly bonded macromolecules with numerous degrees of conformational freedom with various angles between adjacent conjugated monomers, resulting in different chain arrangements varying from completely amorphous, semiordered, to crystalline structures.[5−10] In this regard, the capacity to control the degree of chain order and molecular conformation is a key component to exploit the anisotropic properties of these materials. Previously, the planar conformation adopted by some conjugated polymers was investigated as an alternative to achieve molecular alignment and regular molecular crystalline structure in solid-state systems.[11−13] These rigid coplanar structures in the solid state can also increase the effective conjugation length and suppress the nonradiative decay and excited polaron formation with improved photon absorption and emission properties.[14−16] In this work, our interest is to

Received: November 28, 2017
Accepted: January 3, 2018
Published: January 3, 2018

DOI: 10.1021/acs.jpclett.7b03148
J. Phys. Chem. Lett. 2018, 9, 364−372

Scheme 1. General Chemical Structures of Two Generation Polyfluorenes in the Previous Works That Could Be Induced To Adopt a β-Conformation[a]

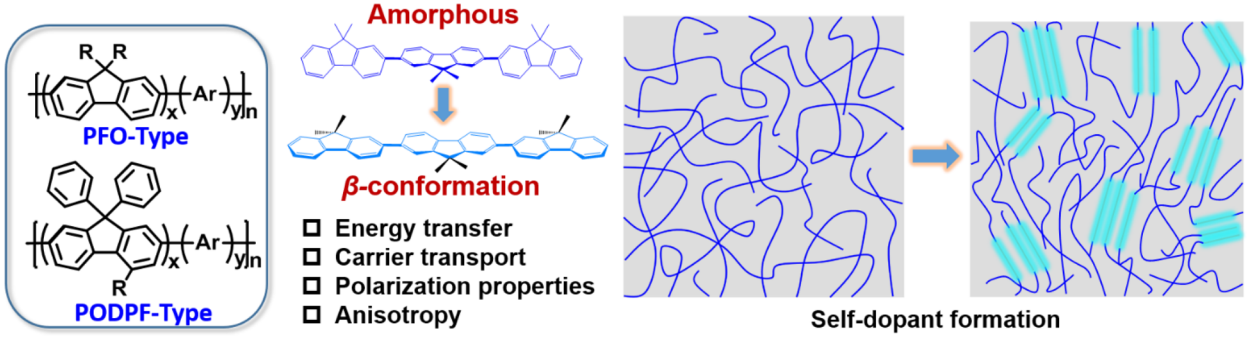

[a]Schematic illustrations of dihedral angle and film orderliness in the amorphous and β-conformation film.[22]

explore the effect of planar conformational transition and chain oriented arrangement in a conjugated polymer on the photophysical and anisotropic properties studied via time-resolved and steady-state spectroscopic measurements.

Among all light-emitting conjugated polymers, polyfluorenes (PFs) exhibit intriguing conformation-induced polymorphic behaviors, involving mainly two kinds of chain conformations, namely, the glassy and β-conformation states, respectively. These enable the conformation-dependent photophysical properties of conjugated polymers to be investigated in detail.[1,9,17−20] The coplanar β-conformation, which is endowed with longer effective conjugated length, effective intra/intermolecular charge transport, high-density molecular stacking, and highly anisotropic properties, is a promising way to form ordered and oriented structures that can result in improved carrier mobility, polarized emission, excellent spectral stability, and enhanced device efficiency.[21−25] On the contrary, the coexistence of diverse chain conformations or multiphases in the film states likely induces inhomogeneous morphologies, which significantly affects the dynamics of electron/hole transport and device performance.[6,26−28] The nature of these spatial areas or connections in various conformations, phases, or aggregates is poorly understood and should be the subject of further study. Despite extensive investigations, the precise conformational behavior, photophysical processes, and anisotropic properties of polyfluorenes have remained elusive. Moreover, analysis of the time-resolved emission behavior of the diverse conformations, especially in terms of excitonic behavior, have been discussed in many literature articles, but the interpretation of these observations is still controversial.[14,29−33] Furthermore, the interplay between the diverse conformations adopted and the anisotropic properties in conjugated polymers is far from being clearly articulated. One difficulty originates from these conformations' intermediate location on the oriented-disorder scale in these inhomogeneous films. High-resolution optical spatiotemporal microscopy methods are a useful tool to provide this spatial information.[34] Coupling ultrafast spectroscopic visualization methods with high spatial resolution optical techniques makes it possible to map the dynamics of the photoinduced charge-transfer/transport processes as a function of location in the film. In this letter, we systematically explored the fluorescence dynamics and anisotropic property of polyfluorenes exhibiting diverse conformation (glassy (α-, amorphous) and β-conformation) behaviors in inhomogeneous self-doped films[22] on submicrometer spatial and picosecond temporal scales using time-resolved scanning confocal fluorescence imaging (FLIM) and fluorescence anisotropy imaging microscopy (FAIM) measurements. Our results show that the fluorescence decay characteristics of the diverse conformations adopted can be determined via FLIM. The use of FAIM in polyfluorene films with and without β-conformation is also explored here to monitor their change upon the conformation transition. Interestingly, our polyfluorene β-conformation films also show ultrastable amplified spontaneous emission (ASE) with a relatively low threshold.

In recent years, numerous efforts have been made to investigate the effects of molecular characteristics, such as molecular weight,[35] alkyl substituent,[36] and copolymer structure,[37,38] on the formation of the β-conformation in polyfluorenes. A mechanism of the β-conformation formation has been proposed, where the interactions between the side chains provide the chemical energy to overcome the activation energy barrier and planarize the polymer backbone, leading to the extended conjugation length that characterizes the β conformation.[23,36,39] Therefore, the prerequisite to achieve efficient adoption of the β-conformation is the van der Waals (VDW) forces of alkyl side chains must be strong enough to overcome the steric repulsion and planarize the polymer backbone.[36] The delicate balance would be easily destroyed by the introduction of molecular segments at higher copolymerized fractions. Previous researcher have revealed that two types of polyfluorenes could induce the formation of the β-conformation, namely, polydialkylfluorene (PDAF) (first-generation) and polydiarylfluorenes (second-generation) derivatives (Scheme 1).[23,37,38,40,41] An optimal chain length for the formation of β-conformation in polyfluorene derivatives is regarded as an octyl side chain on the type polyfluorenes groups, through which it is easier to form the required interdigitation packing than any other length and substituted style.[36,41] In addition, most literature examples show that the low-content β-conformation of PDAFs is only retained after the introduction of copolymerized units, chiral groups, cross-linking networks, or surfactant zwitterion groups.[37,38,42,43]

In general, this coplanar conformation in conjugated polymers induces longer effective conjugated lengths, which may induce an extra shoulder in the absorption spectra and red-shifted PL spectra.[28,44] Therefore, the polyfluorenes' β-conformation is very characteristic in optical spectroscopy. For example, a new absorption shoulder peak at 430−445 nm, below the π-π* transition, is attributed to the polyfluorene β-conformation. The β-conformation of poly(9,9-dioctylfluorene-

DOI: 10.1021/acs.jpclett.7b03148
J. Phys. Chem. Lett. 2018, 9, 364−372

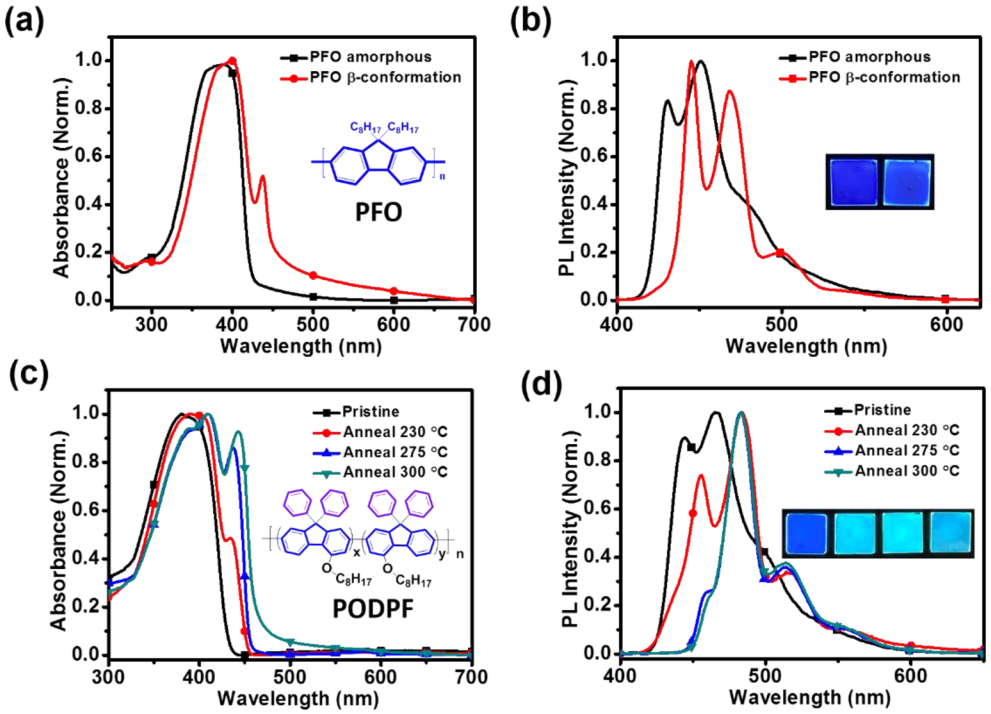

Figure 1. (a) UV−vis and (b) PL spectra of PFO amorphous and β-conformation films spin-coated from $CHCl_3$ and DCE solutions, respectively, the inset showing the molecular structure of PFO and a photograph of PFO films with and without β-conformation under 365 nm UV lamp. (c) UV−vis and (d) PL spectra of PODPF films before and after annealing at 230, 275, and 300 °C, the inset showing the molecular structure of PODPF and a photograph of corresponding films under 365 nm UV lamp.

2,7-diyl) (PFO) also produces marked changes in the emission spectrum, where the structured and red-shifted emission of the β-conformation dominates, even for very small copolymer fractions. The domination of the β-conformation emission comes about through efficient Förster transfer from the "host" α-conformational chain to the β-conformation inclusions (or guests) in the amorphous matrix,[9,22,45,46] which induced self-dopant film formation (Scheme 1). According to previous work, time-resolved energy-transfer measurements show this transfer to be a very efficient process (~5 ps) in PFO-type materials.[14] β-Conformation emission is characterized by a spectrum of very well-defined sharp vibronic replicas with almost no Stokes shift. Indeed, the spectrum is very similar to that of a ladder polymer.[47,48]

As shown in Figure 1a, the absorption spectrum of the PFO film spin-coated from $CHCl_3$ solution shows a maximum at 382 nm, and the corresponding emission peaks appear at 430, 450, and 482 nm, suggesting the amorphous state. The β-conformation of PFO is planar with an extended effective conjugation length, which can be probed by the characteristic shoulder in the normalized absorption spectrum at 437 nm in addition to the main peak at 394 nm (Figure 1a).[49,50] The PL spectrum exhibits three emission bands with peaks at 445, 468, and 499 nm, corresponding to 0−0, 0−1, and 0−2 vibrational transition of the β-conformation, respectively, which is ascribed to efficient energy transfer from the amorphous region to β-domains (Figure 1b). The inset in Figure 1b shows the color of the deep-blue film turning to sky blue after conformational transition under UV lamp irradiation at 365 nm. The detailed optical properties are listed in Table S1. PODPF in the β-conformation could be obtained via post-treatment of a pristine amorphous film after thermal annealing at temperatures above 220 °C. As shown in Figure 1c,d, for the pristine film, the maximum absorption peak is at 385 nm, and the PL spectrum exhibits three emission bands at 445, 466, and 499 nm, indicative of the amorphous state. However, dramatic differences appeared after thermal annealing. An absorption shoulder peak appears at 434 nm following annealing the pristine film at 230 °C, which was similar to the characteristic absorption peak of the PFO β-conformation. With increasing annealing temperature, the intensity of the shoulder peak increased, indicating an enhanced content of β-conformation. A new peak at 409 nm in the absorption spectra of films annealed at 275 and 300 °C indicates the presence of strong chain aggregation resulting from chain rearrangement under thermal activation, where the α-chains transferred into planar conformation. The absorption spectrum of the film annealed at 300 °C exhibits a prominent additional peak at 443 nm, and the intensity in the wavelength range of 457 to 550 nm increased compared with the other three profiles, which demonstrates that ordered crystalline structure in the film leads to strong self-absorption and light scattering. In terms of emission spectra, the films after annealing treatment exhibit four emission bands at 457, 483, 514, and 556 nm (Figure 1d). Similar to previous work,[22] excitation wavelength-independent PL spectra of PODPF and PFO also confirmed the self-dopant formation in β-conformation film (Figure S1). The inset of Figure 1d illustrates that the film changes from blue to green under UV lamp (365 nm) irradiation, indicating that the chain coplanar conformation of polyfluorene can be obtained both in the PFO spin-coated film from DCE solution and in PODPF thermally annealed films.

According to previous reports, Raman spectroscopy can be used to investigate the conformational transition of polyfluorenes, which is reflected from the vibrational frequencies and intensities.[20,51] As shown in Figure S2, further evidence of PFO

DOI: 10.1021/acs.jpclett.7b03148
J. Phys. Chem. Lett. 2018, 9, 364−372

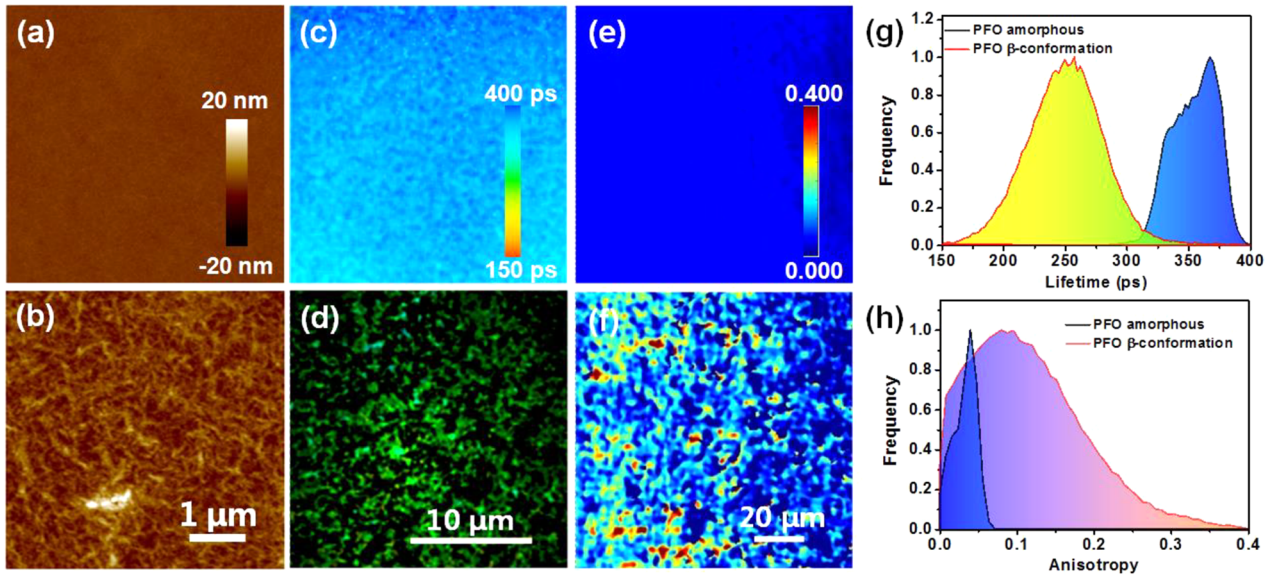

Figure 2. AFM images of PFO films spin-coated from (a) $CHCl_3$ and (b) DCE solution, respectively; the size of the AFM images is 5 μm × 5 μm. FLIM images of PFO (c) amorphous (α-) and (d) β-conformation film. FAIM images of PFO (e) amorphous and (f) β-conformation film. (g) Fluorescence lifetime distributions and (h) fluorescence anisotropy distribution histograms of PFO amorphous and β-conformation films. Two film thickness are both about 100−105 nm.

main-chain complanation is provided by the increasing ratio of the peaks at 1257/1600 cm^{-1}. The frequency of the C−C stretching motion from within the monomer unit of PFO shifts from 1345 to 1349 cm^{-1} between the amorphous and β-conformation forms. The frequency of the C = C stretching motion at ∼1604 cm^{-1} was slightly soft-shifted, ascribed to the longer conjugation length owing to the planar conformation, compared with that of the twisted structure. Similar spectral changes can be seen in the Raman spectra representing the PODPF conformational transition. Comparing the data of Figure S3 with our previous report, the characteristic peaks can be used to probe the planar conformation.[21] The intensity ratio of the 1303/1600 cm^{-1} peaks increases significantly with increasing content of β-conformation. A 4 cm^{-1} hard shift from 1351 to 1355 cm^{-1}, attributed to the frequency of the C−C stretching motion, occurred in PODPF. The soft shift 9 cm^{-1} of C═C stretching motion (from 1601 to 1592 cm^{-1}) is another sign of planar conformation.

The atomic force microscopy images of PFO films spin-coated from $CHCl_3$ and DCE solutions (Figure 2a,b, respectively) illustrate the change in morphology between the α- and β-conformation films. The α-conformation film is uniform and smooth, which is consistent with previously reported amorphous films.[25,46] Significant differences between the two films are also observed in their time-resolved fluorescence images (Figure 2c,d) and the corresponding average fluorescence lifetime histograms (Figure 2g). The FLIM image of the film cast from $CHCl_3$ is homogeneous without any indication of large aggregates and domains. The average fluorescence lifetime distribution of the amorphous film was reasonably narrow peaking at ∼370 ps. These emission decay times are in general agreement with those typically reported for PFO solutions and films recorded in large area illumination (ensemble averaged) measurements. In contrast, the film cast from DCE solution exhibited a root-mean-square (RMS) roughness (2.15 nm) in the AFM image (Figure 2b), significantly higher than that of the amorphous sample, corresponding to marked topographical structure. The increased roughness was ascribed to the chains' aggregation in a solvent (DCE) of moderate quality for this material.[46] The high β-conformation content is further represented by an increase in the inhomogeneity of the lifetime map on micro- and submicrometer scales in the FLIM image (Figure 2d) in keeping with the results of AFM analysis[25,46] and a significant change in the corresponding average fluorescence lifetime histogram (Figure 2g) that shifts to shorter (150−350 ps, with peak at ∼253 ps) times and becomes more uniformly distributed. The chain planarization therefore leads to a marked decrease in the fluorescence lifetime and slightly lowered quantum yield.

Films comprising molecular aggregates or crystalline structures can be viewed as a "self-doped" system[22] where a fraction of chains with a lower energy gap are intimately dispersed within a "matrix" of more amorphous polymer chains with a larger energy gap. According to previous work,[14] the excitons photogenerated in the amorphous matrix of PFO film surrounding the β-conformation chains can transfer to the lower energy β-conformation chains on very rapid (shorter than ∼5 ps) time scales, which is shorter than the temporal resolution of our detector. Energy migration can, however, be visualized by fluorescence anisotropy imaging (FAIM). FAIM reports on the difference between fluorescence intensities emitted parallel and perpendicular to the plane of polarization of the excitation light that result from emission depolarizing processes occurring within the excited-state lifetime.[52,53] In the absence of rotational diffusion of chromophores, fluorescence depolarization can result from the randomization of the orientation of the emission transition dipole, relative to the absorption transition dipoles of the initially photoselected chromophore, following steps of Förster-mediated energy migration.[54,55] The FAIM images of the amorphous and β-conformation films (Figure 2e,f, respectively) illustrate a marked difference in the degree of emission depolarization that is quantified in the fluorescence anisotropy histograms calculated on a pixel-by-pixel basis (Figure 2h). The uniformity of the FAIM image and the reasonably narrow corresponding

DOI: 10.1021/acs.jpclett.7b03148
J. Phys. Chem. Lett. 2018, 9, 364−372

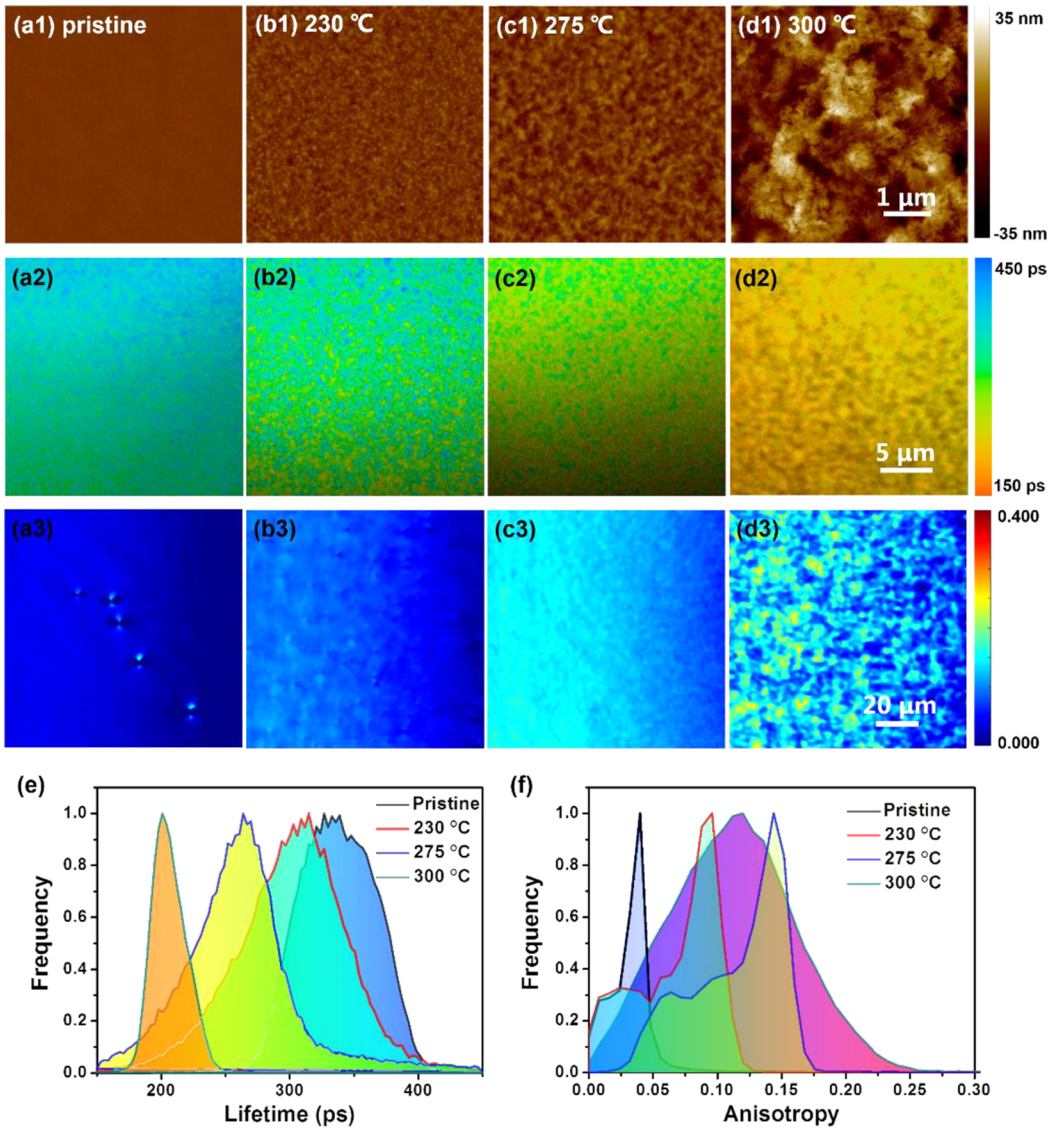

Figure 3. Atomic force microscopy (AFM) images of PODPF films (a) before annealing and after annealing at (b) 230, (c) 275, and (d) 300 °C; the size of the AFM images is 5 μm × 5 μm. (a2−d2) FLIM and (a3−d3) FAIM images of corresponding films. (e) Average fluorescence lifetime and (f) fluorescence anisotropy distribution histograms of PODPF films following annealing at different temperatures. All film thickness are about 105−110 nm.

anisotropy distribution of the amorphous film (deep blue) reflect the homogeneous morphology seen in both the other microscopy modes. In comparison, the FAIM image of the PFO β-conformation film (Figure 2f) shows some pixels of high anisotropy values (red), with many exhibiting quite low anisotropy values (dark blue), corresponding to high and low degrees of emission depolarization, respectively. The fluorescence anisotropy distribution (Figure 2h) is correspondingly broader and centered at higher anisotropy values than that of the amorphous film. These observations reflect the heterogeneous environment within the β-conformation film, which comprises aggregated domains, with short emission decay times and variable emission depolarization attributed to energy transfer/migration from the amorphous state to the β-conformation. According to PFO absorption spectra in Figure 1a, the fraction of β-conformation in this PFO film is estimated roughly by subtracting the contribution from the amorphous state in the absorption spectrum, and the calculation result is ~39.5% (Figure S4), which is largely in agreement with the results of the FLIM and FAIM images. As we know, this is the first to provide a direct visualization to screen the self-dopant in PFO β-conformation films.

To confirm our assumption above, we also systematically explored the photophysical properties of second-generation β-polyfluorene, PODPF, in various conformations using the same methods. The β-conformation can often be obtained in films following post-treatment, such as solvent and thermal annealing. Owing to the chemical oxidation, chain aggregation, and morphological instability (lower glass- and crystallization-transition temperature, T_g = 65 °C, T_c = 120 °C), the PFO β-conformation films cannot be widely applied in optoelectrical device. In contrast, our PODPF material shows intrinsically high chemical stability in air, so we can precisely tune the fraction of β-conformation in the film states via controlling the thermal annealing temperature. First, a homogeneous morphology is observed in the AFM image of the pristine amorphous film (Figure 3a1),[21,41] suggesting excellent film-forming stability and homogeneous morphology similar to the PFO

DOI: 10.1021/acs.jpclett.7b03148
J. Phys. Chem. Lett. 2018, 9, 364−372

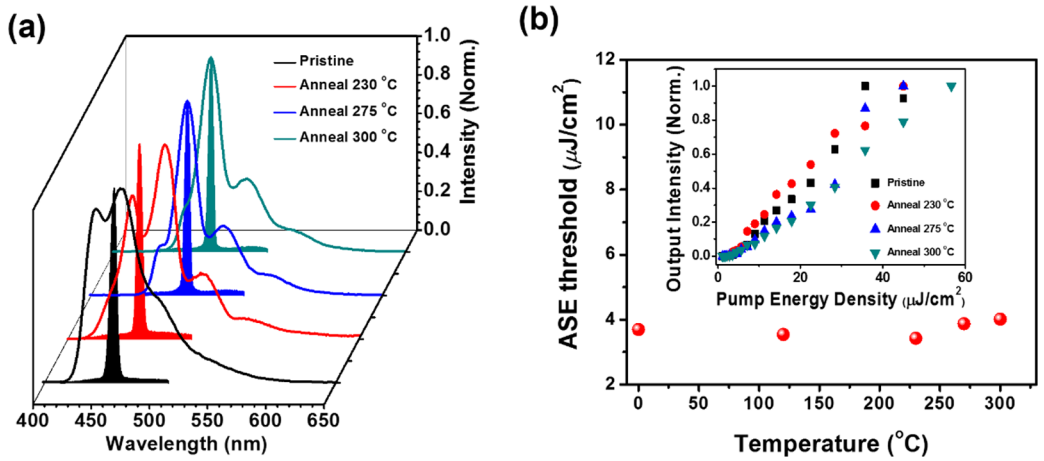

Figure 4. (a) Normalized PL and ASE spectra (excited at 380 nm) of the PODPF various spin-coated films. (b) Thermal annealing temperature dependence of the ASE threshold; inset shows the ASE output intensity versus pump energy density.

pristine film. This is confirmed by the FLIM image and corresponding average fluorescence lifetime distribution (Figure 3e). The lifetimes of the amorphous film range from 250 to 420 ps with a peak of ~335 ps, similar to the behavior of the PFO amorphous film spin-coated from $CHCl_3$ solution discussed above. By annealing the pristine film at 230 °C for 10 min, the roughness increased to 1.79 nm, and several small "granular" domains appeared with a size of tens of nanometers (~20 nm, Figure 3b1). Some amounts of β-conformation (~21.8%, Figure S5) were found as well, according to the absorption and PL spectra. As the annealing temperature is increased, more and larger granular (~100−800 nm) structures appeared (Figure 3c1,d1), while simultaneously more β-conformation (~45.8%), according to the absorption spectra in Figure 1c, was obtained. The increasingly rough topography is attributed to chain aggregation, which was confirmed by the stronger absorption peak at 409 nm, and the aggregation induced conformational transition.[41] In fact, the shoulder absorption peak of this film is ~443 nm, red-shifted about 6−9 nm compared with those of pristine film thermal annealed at 230 or 275 °C. The FLIM images (Figure 3a2−d2,e) illustrate that as larger domains form with increasing annealing temperature, the average fluorescence decay lifetimes become significantly shorter. The tendency of emission decay times to decrease in PODPF as the β-conformation forms is similar to PFO. It is noteworthy that the film morphology obtained following thermal annealing at 300 °C is significantly different from the other three samples. Such high temperature is close to the melting point (310 °C) of PODPF, which activates the chains motion most dramatically, causing the maximum aggregation or crystallization of the chains. The morphology adopted following annealing at this temperature also corresponded to the shortest and narrowest decay time distribution.

The fluorescence anisotropy distribution plots (Figure 3f) calculated from the FAIM images (Figure 3a3−d3) indicate that the emission is markedly more polarized and oriented after annealing at the lower two temperatures compared with the pristine film. The unique behavior of the film annealed at 300 °C compared with the lower temperatures is also evident from the FAIM analysis, with the anisotropy distribution centering at an intermediate anisotropy value and being far broader than the other distributions. The low fluorescence anisotropy exhibited by the pristine film is consistent with completely random chain packing inferred from the AFM and FLIM images. After thermal annealing at 230 and 275 °C, the increase in the peak anisotropy value is indicative of increased order (crystallinity) within the film, resulting in a higher degree of emission within one plane of polarization. The higher degree of order is consistent with the increased absorption at 409 nm (Figure 1c)[41] attributed to the increased chain crystallization than those of PODPF film with lower fraction β-conformation and PFO β-conformation spin-coated from DCE solution. However, these fluorescence anisotropy maps and their anisotropy distribution plots show that some level of disorder remains within these films, indicated by the shoulder in the histograms to lower values of fluorescence anisotropy. The broad anisotropy distribution of the sample containing the highest level of PODPF β-conformation (thermal annealed at 300 °C) reflects a heterogeneous environment comprising mixed amorphous and β-conformation regions (amorphous, crystalline, and other phase) in the film.

In fact, this regular and oriented chain arrangement in the condensed state is a prerequisite for the construction of electrical pump laser. Unfortunately, the intrinsic aggregation behavior and oxidation property of first-generation β-polyfluorenes, PFO-type, limited their wide practical optoelectronic applications. Therefore, with a combination of high photoluminescence quantum yield (PLQY) and good thermal and spectral stability, we focused on further investigating the possibility of PODPF as the gain medium in an organic solid-state laser in this work.[21,23,40] Fortunately, according to our previous work,[21] PODPF β-conformational film exhibited relative higher charge mobility up to 10^{-3} cm^2/V s, and the influence of the oriented β-conformation on the ASE characteristics was studied using a Q-switched Nd^{3+}:YAG laser operating as the pump source at a wavelength near the polymer absorption maximum. As shown in Figure 4a, upon optical pumping, all samples show prominent ASE from the 0−1 vibration transition, with the peak wavelength centered at ~463 nm for the pristine film and film after thermal annealed at 230 °C. However, similar to our previous work,[21] β-conformational film obtained after thermal annealing at 275 and 300 °C exhibited a ASE peak at 483 nm. Interestingly, the ASE threshold of all our PODPF films was found to be similarly relative lower under the same experimental conditions (Figure 4b). Notably, all our samples showed a low ASE threshold of 41.24 nJ/pulse (3.42 $\mu J/cm^2$) to 48.36 nJ/pulse (4.01 $\mu J/cm^2$), which is the comparable lower threshold of the fluorene-based

DOI: 10.1021/acs.jpclett.7b03148
J. Phys. Chem. Lett. 2018, 9, 364−372

polymer or macromolecule (similar ASE peaks) and the metal-halide perovskites.[40,56,57] The ASE characteristics were measured as a function of gradient annealing temperature to investigate the thermal stability of the gain property. Actually, it is easy to observe that there is no change in the threshold of all samples with increasing the annealing temperature from room temperature to even 300 °C. In this regard, we believed that PODPF is an effective and potential gain medium for the organic laser, especially electrical pump laser. We also make an attempt to fabricate PODPF-patterned nanostructure for organic nanolaser and nanophotonic elements via controlling laser-beam induced conformation transition in situ.[24]

In conclusion, we systematically investigated the photophysical and fluorescence anisotropic behavior of polyfluorene amorphous and β-conformation, prepared either as a function of solvent or annealing temperature, respectively. Variations in the level of β-conformational polyfluorenes influence the absorption and emission spectra, emission decay properties, morphology, and fluorescence anisotropy of the film. The excitons of the β-conformation decay faster than those in the amorphous state. The fluorescence anisotropy of conjugated polymers can report on the level of order within the film, which can be varied by controlling chain conformations via solvent or thermal methods. Ultrastable ASE property of PODPF with the lower threshold of 3.42 $\mu J/cm^2$ also confirms the potential practical application in organic lasers. Such simple approaches will find broad applications in nanostructured, polymeric optoelectronic thin film systems.

■ ASSOCIATED CONTENT

Supporting Information

The Supporting Information is available free of charge on the ACS Publications website at DOI: 10.1021/acs.jpclett.7b03148.

Experimental section. Figure S1. PL spectra of PFO β-conformation films spin-coated from DCE solution and PODPF films annealed at 300 °C, with different excitation wavelengths. Figure S2. Raman spectra of PFO films with amorphous and β-conformation. Figure S3. Raman spectra of PODPF with different content of β-conformation in self-doped films. Figure S4. Comparison of the PFO absorption spectra obtained from the DCE spin-coated film with the spectra from the individual β-conformation and amorphous state. Figure S5. Comparison of the PODPF absorption spectra obtained from annealed films at 230, 275, and 300 °C with the spectra from the individual β-conformation and amorphous state. Table S1-1. Summary of basic optical spectra of PFO. Table S1-2. Summary of basic optical spectra of PODPF. (PDF)

■ AUTHOR INFORMATION

Corresponding Authors

*J.-Y.L.: E-mail: iamjylin@njtech.edu.cn.
*T.A.S.: E-mail: trevoras@unimelb.edu.au.
*L.-H.X.: E-mail: iamlhxie@njupt.edu.cn.
*W.H.: E-mail: wei-huang@njtech.edu.cn.

ORCID

Rui-Dong Xia: 0000-0003-4123-9096
Ling-Hai Xie: 0000-0001-6294-5833
Wei Huang: 0000-0001-7004-6408

Notes

The authors declare no competing financial interest.

■ ACKNOWLEDGMENTS

The project was supported by the National Key Basic Research Program of China (973) (2015CB932200), the National Natural Science Foundation of China (U1301243, 21274064, 21504041), Doctoral Fund of Ministry of Education of China (20133223110007), Project Funded by the Priority Academic Program Development of Jiangsu Higher Education Institutions, PAPD (YX03002), the Six Peak Talents Foundation of Jiangsu Province (XCL-CXTD-009), and Program for Postgraduates Research Innovation in University of Jiangsu Province (KYCX17_0752). We also acknowledge support by the International Research and Research Training Fund (IRRTF) from the University of Melbourne and the ARC Centre of Excellence in Exciton Science (CE170100026). J.L. also acknowledges SICAM Fellowship (NanjingTech), the Plastic Electronics Centre, Physics Department of Imperial College London (IC), and Oxford University.

■ REFERENCES

(1) Xie, L. H.; Yin, C. R.; Lai, W. Y.; Fan, Q. L.; Huang, W. Polyfluorene-based semiconductors combined with various periodic table elements for organic electronics. *Prog. Polym. Sci.* **2012**, *37*, 1192−1264.

(2) Heeger, A. J. Semiconducting polymers: the Third Generation. *Chem. Soc. Rev.* **2010**, *39*, 2354−2371.

(3) Monkman, A.; Rothe, C.; King, S.; Dias, F. Polyfluorene photophysics. *Adv. Polym. Sci.* **2008**, *212*, 187−225.

(4) Grell, M.; Bradley, D. D. C. Polarized luminescence from oriented molecular materials. *Adv. Mater.* **1999**, *11*, 895−905.

(5) Kim, B. G.; Jeong, E. J.; Chung, J. W.; Seo, S.; Koo, B.; Kim, J. A molecular design principle of lyotropic liquid-crystalline conjugated polymers with directed alignment capability for plastic electronics. *Nat. Mater.* **2013**, *12*, 659−664.

(6) Noriega, R.; Rivnay, J.; Vandewal, K.; Koch, F. P. V.; Stingelin, N.; Smith, P.; Toney, M. F.; Salleo, A. A general relationship between disorder, aggregation and charge transport in conjugated polymers. *Nat. Mater.* **2013**, *12*, 1038−1044.

(7) Knaapila, M.; Monkman, A. P. Methods for Controlling Structure and Photophysical Properties in Polyfluorene Solutions and Gels. *Adv. Mater.* **2013**, *25*, 1090−1108.

(8) Lin, J. Y.; Liu, B.; Yu, M. N.; Ou, C. J.; Lei, Z. F.; Liu, F.; Wang, X. H.; Xie, L. H.; Zhu, W. S.; Ling, H. F.; Zhang, X. W.; Stavrinou, P. N.; Wang, J. P.; Bradley, D. D. C.; Huang, W. Understanding the molecular gelation processes of heteroatomic conjugated polymers for stable blue polymer light-emitting diodes. *J. Mater. Chem. C* **2017**, *5*, 6762−6770.

(9) Yu, M. N.; Liu, B.; Lin, J. Y.; Li, T.; Lu, D.; Liu, F.; Zhu, W. S.; Xie, L. H.; Huang, W. Nondilute 1,2-dichloroethane solution of poly(9,9-dioctylfluorene-2,7-diyl): A study on the aggregation process. *Chin. J. Polym. Sci.* **2016**, *34*, 1311−1318.

(10) Lin, J. Y.; Yu, Z. Z.; Zhu, W. S.; Xing, G. C.; Lin, Z. Q.; Yang, S. H.; Xie, L. H.; Niu, C. L.; Huang, W. A π-conjugated polymer gelator from polyfluorene-based poly(tertiary alcohol) via the hydrogen-bonded supramolecular functionalization. *Polym. Chem.* **2013**, *4*, 477−483.

(11) Torkkeli, M.; Galbrecht, F.; Scherf, U.; Knaapila, M. Solid State Structure of Poly(9,9-dinonylfluorene). *Macromolecules* **2015**, *48*, 5244−5250.

(12) Knaapila, M.; Torkkeli, M.; Galbrecht, F.; Scherf, U. Crystalline and Noncrystalline Forms of Poly(9,9-diheptylfluorene). *Macromolecules* **2013**, *46*, 836−843.

(13) Chen, S. H.; Chou, H. L.; Su, A. C.; Chen, S. A. Molecular packing in crystalline poly(9,9-di-n-octyl-2,7-fluorlene). *Macromolecules* **2004**, *37*, 6833−6838.

DOI: 10.1021/acs.jpclett.7b03148
J. Phys. Chem. Lett. 2018, 9, 364−372

(14) Ariu, M.; Sims, M.; Rahn, M. D.; Hill, J.; Fox, A. M.; Lidzey, D. G.; Oda, M.; Cabanillas-Gonzalez, J.; Bradley, D. D. C. Exciton migration in β-phase poly(9,9-dioctylfluorene). *Phys. Rev. B: Condens. Matter Mater. Phys.* **2003**, *67*, 195333.
(15) Collini, E.; Scholes, G. D. Coherent Intrachain Energy Migration in a Conjugated Polymer at Room Temperature. *Science* **2009**, *323*, 369−373.
(16) Shaw, P. E.; Ruseckas, A.; Peet, J.; Bazan, G. C.; Samuel, I. D. W. Exciton-Exciton Annihilation in Mixed-Phase Polyfluorene Films. *Adv. Funct. Mater.* **2010**, *20*, 155−161.
(17) Grell, M.; Bradley, D. D. C.; Inbasekaran, M.; Woo, E. P. A glass-forming conjugated main-chain liquid crystal polymer for polarized electroluminescence applications. *Adv. Mater.* **1997**, *9*, 798−802.
(18) Grell, M.; Bradley, D. D. C.; Ungar, G.; Hill, J.; Whitehead, K. S. Interplay of physical structure and photophysics for a liquid crystalline polyfluorene. *Macromolecules* **1999**, *32*, 5810−5817.
(19) Chunwaschirasiri, W.; Tanto, B.; Huber, D. L.; Winokur, M. J. Chain conformations and photoluminescence of poly(di-n-octylfluorene). *Phys. Rev. Lett.* **2005**, *94*, 107402.
(20) Arif, M.; Volz, C.; Guha, S. Chain morphologies in semicrystalline polyfluorene: Evidence from raman scattering. *Phys. Rev. Lett.* **2006**, *96*, 025503.
(21) Liu, B.; Lin, J. Y.; Liu, F.; Yu, M. N.; Zhang, X. W.; Xia, R. D.; Yang, T.; Fang, Y. T.; Xie, L. H.; Huang, W. A Highly Crystalline and Wide-Bandgap Polydiarylfluorene with β-Phase Conformation toward Stable Electroluminescence and Dual Amplified Spontaneous Emission. *ACS Appl. Mater. Interfaces* **2016**, *8*, 21648−21655.
(22) Lu, H. H.; Liu, C. Y.; Chang, C. H.; Chen, S. A. Self-dopant formation in poly(9,9-di-n-octylfluorene) via a dipping method for efficient and stable pure-blue electrolumineseence. *Adv. Mater.* **2007**, *19*, 2574−2579.
(23) Lin, J. Y.; Zhu, W. S.; Liu, F.; Xie, L. H.; Zhang, L.; Xia, R. D.; Xing, G. C.; Huang, W. A Rational Molecular Design of β-Phase Polydiarylfluorenes: Synthesis, Morphology, and Organic Lasers. *Macromolecules* **2014**, *47*, 1001−1007.
(24) Perevedentsev, A.; Sonnefraud, Y.; Belton, C. R.; Sharma, S.; Cass, A. E. G.; Maier, S. A.; Kim, J. S.; Stavrinou, P. N.; Bradley, D. D. C. Dip-pen patterning of poly (9,9-dioctylfluorene) chain-conformation-based nano-photonic elements. *Nat. Commun.* **2015**, *6*, 5977.
(25) Zhang, X. W.; Hu, Q.; Lin, J. Y.; Lei, Z. F.; Guo, X.; Xie, L. H.; Lai, W. Y.; Huang, W. Efficient and stable deep blue polymer light-emitting devices based on β-phase poly(9,9-dioctylfluorene). *Appl. Phys. Lett.* **2013**, *103*, 153301.
(26) Spano, F. C.; Silva, C. H- and J-Aggregate Behavior in Polymeric Semiconductors. *Annu. Rev. Phys. Chem.* **2014**, *65*, 477−500.
(27) Schmidt, K.; Tassone, C. J.; Niskala, J. R.; Yiu, A. T.; Lee, O. P.; Weiss, T. M.; Wang, C.; Frechet, J. M. J.; Beaujuge, P. M.; Toney, M. F. A Mechanistic Understanding of Processing Additive-Induced Efficiency Enhancement in Bulk Heterojunction Organic Solar Cells. *Adv. Mater.* **2014**, *26*, 300−305.
(28) Liu, Y. H.; Zhao, J. B.; Li, Z. K.; Mu, C.; Ma, W.; Hu, H. W.; Jiang, K.; Lin, H. R.; Ade, H.; Yan, H. Aggregation and morphology control enables multiple cases of high-efficiency polymer solar cells. *Nat. Commun.* **2014**, *5*, 5293.
(29) Dias, F. B.; Morgado, J.; Macanita, A. L.; da Costa, F. P.; Burrows, H. D.; Monkman, A. P. Kinetics and thermodynamics of poly(9,9-dioctylfluorene) β-phase formation in dilute solution. *Macromolecules* **2006**, *39*, 5854−5864.
(30) Becker, K.; Lupton, J. M. Dual species emission from single polyfluorene molecules: Signatures of stress-induced planarization of single polymer chains. *J. Am. Chem. Soc.* **2005**, *127*, 7306−7307.
(31) Ariu, M.; Lidzey, D. G.; Sims, M.; Cadby, A. J.; Lane, P. A.; Bradley, D. D. C. The effect of morphology on the temperature-dependent photoluminescence quantum efficiency of the conjugated polymer poly(9, 9-dioctylfluorene). *J. Phys.: Condens. Matter* **2002**, *14*, 9975−9986.
(32) O'Carroll, D.; Iacopino, D.; O'Riordan, A.; Lovera, P.; O'Connor, E.; O'Brien, G. A.; Redmond, G. Poly(9,9-dioctylfluorene) Nanowires with Pronounced β-Phase Morphology: Synthesis, Characterization, and Optical Properties. *Adv. Mater.* **2008**, *20*, 42−48.
(33) Wu, C. F.; McNeill, J. Swelling-Controlled Polymer Phase and Fluorescence Properties of Polyfluorene Nanoparticles. *Langmuir* **2008**, *24*, 5855−5861.
(34) Hao, X. T.; McKimmie, L. J.; Smith, T. A. Spatial Fluorescence Inhomogeneities in Light-Emitting Conjugated Polymer Films. *J. Phys. Chem. Lett.* **2011**, *2*, 1520−1525.
(35) Li, T.; Liu, B.; Zhang, H.; Ren, J. X.; Bai, Z. M.; Li, X. N.; Ma, T. N.; Lu, D. Effect of conjugated polymer poly (9,9-dioctylfluorene) (PFO) molecular weight change on the single chains, aggregation and β-phase. *Polymer* **2016**, *103*, 299−306.
(36) Bright, D. W.; Dias, F. B.; Galbrecht, F.; Scherf, U.; Monkman, A. P. The Influence of Alkyl-Chain Length on β-Phase Formation in Polyfluorenes. *Adv. Funct. Mater.* **2009**, *19*, 67−73.
(37) Lee, S. K.; Ahn, T.; Park, J. H.; Jung, Y. K.; Chung, D. S.; Park, C. E.; Shim, H. K. β-Phase formation in poly(9,9-di-n-octylfluorene) by incorporating an ambipolar unit containing phenothiazine and 4-(dicyanomethylene)-2-methyl-6-p-(dimethylamino)styryl-4H-pyran. *J. Mater. Chem.* **2009**, *19*, 7062−7069.
(38) Bright, D. W.; Moss, K. C.; Kamtekar, K. T.; Bryce, M. R.; Monkman, A. P. The β-Phase Formation Limit in Two Poly(9,9-di-n-octylfluorene) based Copolymers. *Macromol. Rapid Commun.* **2011**, *32*, 983−987.
(39) Lin, Z. Q.; Shi, N. E.; Li, Y. B.; Qiu, D.; Zhang, L.; Lin, J. Y.; Zhao, J. F.; Wang, C.; Xie, L. H.; Huang, W. Preparation and Characterization of Polyfluorene-Based Supramolecular π-Conjugated Polymer Gels. *J. Phys. Chem. C* **2011**, *115*, 4418−4424.
(40) Bai, L. B.; Liu, B.; Han, Y. M.; Yu, M. N.; Wang, J.; Zhang, X. W.; Ou, C. J.; Lin, J. Y.; Zhu, W. S.; Xie, L. H.; Yin, C. R.; Zhao, J. F.; Wang, J. P.; Bradley, D. D. C.; Huang, W. Steric-Hindrance-Functionalized Polydiarylfluorenes: Conformational Behavior, Stabilized Blue Electroluminescence, and Efficient Amplified Spontaneous Emission. *ACS Appl. Mater. Interfaces* **2017**, *9*, 37856−37863.
(41) Liu, B.; Lin, J. Y.; Yu, M. N.; Li, B.; Xie, L. H.; Ou, C. J.; Liu, F.; Li, T.; Lu, D.; Huang, W. Hereditary Character of Alkyl-Chain Length Effect on β-Phase Conformation from Polydialkylfluorenes to Bulky Polydiarylfluorenes. *J. Phys. Chem. C* **2017**, *121*, 19087−19096.
(42) Kuehne, A. J. C.; Mackintosh, A. R.; Pethrick, R. A. β-phase formation in a crosslinkable poly(9,9-dihexylfluorene). *Polymer* **2011**, *52*, 5538−5542.
(43) Zhao, S.; Liang, J. F.; Guo, T.; Wang, Y.; Chen, X.; Fu, D. H.; Xiong, J. B.; Ying, L.; Yang, W.; Peng, J. B.; Cao, Y. Formation of poly(9,9-dioctylfluorene) β-phase by incorporating aromatic moiety in side chain. *Org. Electron.* **2016**, *38*, 130−138.
(44) Liu, B.; Lin, J. Y.; Lei, Z. F.; Sun, M. L.; Xie, L. H.; Xue, W.; Yin, C. R.; Zhang, X. W.; Huang, W. Solvent and Steric Hindrance Effects of Bulky Poly(9,9-diarylfluorene)s on Conformation, Gelation, Morphology, and Electroluminescence. *Macromol. Chem. Phys.* **2015**, *216*, 1043−1054.
(45) Peet, J.; Brocker, E.; Xu, Y. H.; Bazan, G. C. Controlled β-phase formation in poly(9,9-di-n-octylfluorene) by processing with alkyl additives. *Adv. Mater.* **2008**, *20*, 1882−1885.
(46) Ling, H. F.; Lin, J. Y.; Yi, M. D.; Liu, B.; Li, W.; Lin, Z. Q.; Xie, L. H.; Bao, Y.; Guo, F. N.; Huang, W. Synergistic Effects of Self-Doped Nanostructures as Charge Trapping Elements in Organic Field Effect Transistor Memory. *ACS Appl. Mater. Interfaces* **2016**, *8*, 18969−18977.
(47) Wu, Y. G.; Zhang, J. Y.; Fei, Z. P.; Bo, Z. S. Spiro-Bridged Ladder-Type Poly(p-phenylene)s: Towards Structurally Perfect Light-Emitting Materials. *J. Am. Chem. Soc.* **2008**, *130*, 7192−7193.
(48) Scherf, U.; Müllen, K. Polyarylenes and poly(arylenevinylenes), 7-A soluble ladder polymer via bridging of functionalized poly(p-phenylene)-precursors. *Macromol. Rapid Commmun.* **2005**, *26*, 1362−1370.
(49) Yu, M. N.; Liu, B.; Lin, J. Y.; Bai, L. B.; Ling, H. F.; Zhu, W. S.; Xie, L. H.; Yi, M. D.; Wang, J. P.; Huang, W. One-step preparation of conjugated homopolymer sub-microspheres via a controllable supra-

DOI: 10.1021/acs.jpclett.7b03148
J. Phys. Chem. Lett. 2018, 9, 364−372

molecular approach toward optoelectronic applications. *RSC Adv.* **2017**, *7*, 14688−14693.
(50) Lin, J. Y.; Liu, B.; Yu, M. N.; Xie, L. H.; Zhu, W. S.; Ling, H. F.; Zhang, X. W.; Ding, X. H.; Wang, X. H.; Stavrinou, P. N.; Wang, J. P.; Bradley, D. D. C.; Huang, W. Heteroatomic Conjugated Polymers and the Spectral Tuning of Electroluminescence via a Supramolecular Coordination Strategy. *Macromol. Rapid Commun.* **2016**, *37*, 1807−1813.
(51) Volz, C.; Arif, M.; Guha, S. Conformations in dioctyl substituted polyfluorene: A combined theoretical and experimental Raman scattering study. *J. Chem. Phys.* **2007**, *126*, 064905.
(52) Soleimaninejad, H.; Chen, M. Z.; Lou, X. D.; Smith, T. A.; Hong, Y. N. Measuring macromolecular crowding in cells through fluorescence anisotropy imaging with an AIE fluorogen. *Chem. Commun.* **2017**, *53*, 2874−2877.
(53) Jameson, D. M.; Ross, J. A. Fluorescence Polarization/Anisotropy in Diagnostics and Imaging. *Chem. Rev.* **2010**, *110*, 2685−2708.
(54) Banal, J. L.; Soleimaninejad, H.; Jradi, F. M.; Liu, M. Y.; White, J. M.; Blakers, A. W.; Cooper, M. W.; Jones, D. J.; Ghiggino, K. P.; Marder, S. R.; Smith, T. A.; Wong, W. W. H. Energy migration in organic solar concentrators with a molecularly insulated perylene diimide. *J. Phys. Chem. C* **2016**, *120*, 12952−12958.
(55) Zhang, B. L.; Soleimaninejad, H.; Jones, D. J.; White, J. M.; Ghiggino, K. P.; Smith, T. A.; Wong, W. W. H. Highly Fluorescent Molecularly Insulated Perylene Diimides: Effect of Concentration on Photophysical Properties. *Chem. Mater.* **2017**, *29*, 8395−8403.
(56) Xing, G. C.; Mathews, N.; Lim, S. S.; Yantara, N.; Liu, X. F.; Sabba, D.; Gratzel, M.; Mhaisalkar, S.; Sum, T. C. Low-temperature solution-processed wavelength-tunable perovskites for lasing. *Nat. Mater.* **2014**, *13*, 476−480.
(57) Jia, Y. F.; Kerner, R. A.; Grede, A. J.; Rand, B. P.; Giebink, N. C. Continuous-wave lasing in an organic-inorganic lead halide perovskite semiconductor. *Nat. Photonics* **2017**, *11*, 784−788.

DOI: 10.1021/acs.jpclett.7b03148
J. Phys. Chem. Lett. 2018, 9, 364−372